Optics Letters

Selective excitation of optical vortex modes with specific charge numbers in band-tuned topological waveguides

Hibiki Kagami,[1,4] Tomohiro Amemiya,[1,2,5] Sho Okada,[1] Yahui Wang,[1] Nobuhiko Nishiyama,[1,2] and Xiao Hu[3]

[1]Department of Electrical and Electronic Engineering, Tokyo Institute of Technology, Tokyo 152-8552, Japan
[2]Institute of Innovative Research (IIR), Tokyo Institute of Technology, Tokyo 152-8552, Japan
[3]International Center for Materials Nanoarchitectonics (WPI-MANA), National Institute for Materials Science, Tsukuba 305-0044, Japan
[4]e-mail: kagami.h.aa@m.titech.ac.jp
[5]e-mail: amemiya.t.ab@m.titech.ac.jp

Received 4 February 2022; revised 14 March 2022; accepted 15 March 2022; posted 15 March 2022; published 19 April 2022

We propose a method for selectively propagating optical vortex modes with specific charge numbers in a photonic integrated circuit (PIC) by using a topological photonic system. Specifically, by performing appropriate band tuning in two photonic structures that comprise a topological waveguide, one specific electromagnetic mode at the Γ point of a band diagram can be excited. Based on theoretical analysis, we successfully propagated optical vortex modes with specific charge numbers over a wide range in the C band in the proposed topological waveguide. The proposed method could be useful in controlling optical vortex signals at the chip level in future orbital angular momentum multiplexing technologies.

https://doi.org/10.1364/OL.454946

The transmission performance of optical networks is determined by three basic technologies: baud rate increase, multi-symbol operations, and multiplexing with some physical parameters. Current optical communication is achieved by combining these technologies. Multiplexing can be of several types, and those already used in the market include wavelength-division multiplexing (WDM) and polarization-division multiplexing (PDM). Recently, transmission of the order of 10–100 Pb/s has been achieved by combining these technologies with spatial multiplexing using multicore fibers [1,2].

In this context, many aspects of optical vortices have not yet been explored, and numerous studies have been conducted so far in this regard [3–6]. The optical vortex carries the orbital angular momentum (OAM) of light and can be used to multiplex signals by assigning each signal to a light wave with a different momentum. Orbital angular momentum is characterized by a wavefront with a helix shape, and the wavefront consists of mutually orthogonal helices with different charge numbers l (the step length of each helix surface is equal to $l\lambda$). This technique has excellent affinity with existing multiplexing technologies such as WDM and PDM, and is becoming an increasingly promising future multiplexing technology [7–15].

However, the affinity with optical vortices is not high in the planar photonic integrated circuits (PICs) that are widely used today in optical communications [16–20] because waveguide devices in a PIC operate only with transverse electric/magnetic-mode light. Therefore, we aim to perform various control operations, including the propagation of optical vortex modes in optical circuits, by replacing parts of conventional optical circuits with topological photonic systems (topological PICs) [21–23].

One of the most well-known phenomena in topological photonic systems is the topological edge state that occurs at the interface between two photonic structures with different topologies, and this phenomenon allows the selective propagation of light with specific internal degrees of freedom [24–28]. Consequently, optical waveguides that exhibit low loss even through sharp bends become feasible; in such lines, information arising from photonic topology such as circularly polarized light (i.e., optical spin) and optical vortices (i.e., orbital angular momentum) is retained. Such lines are hereafter referred to as "topological waveguides" [29–32].

To facilitate the use of the abovementioned phenomenon in future OAM multiplexing technologies, it is expected that topological waveguides capable of propagating optical vortex modes with specific charge numbers (l) in PICs will be developed. In this paper, we propose that it is possible to selectively excite/propagate optical vortex modes with specific charge numbers (l) by performing appropriate band tuning in topological photonic crystals through band analysis using the plane wave expansion (PWE) method. We constructed an optical vortex multiplexing device using the proposed method, and the propagation characteristics were analyzed using the time-domain difference (FDTD) method.

Figure 1(a) shows a schematic band diagram of two photonic structures used in typical topological waveguides. In this case, the band inversion of the electromagnetic mode occurs near the Γ point in the band diagram, which induces the topological edge state at the interface between the two photonic structures with different topologies. Using modes with the same symmetry as

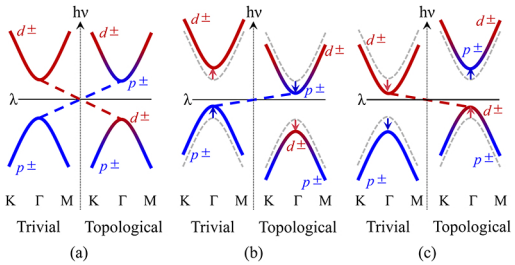

Fig. 1. (a) Schematic band diagram of two photonic structures used for typical topological waveguides. (b), (c) Tuned band diagram of two photonic structures used for specific topological waveguides capable of propagating optical vortex modes with $l = \pm 1$ and $l = \pm 2$.

the atomic orbitals p_z, p_x, d_{zx}, and $d_{z^2-x^2}$, the distribution of the electromagnetic field localized in each lattice forming the topological waveguide can be expressed as follows [26]:

$$p_\pm = \frac{1}{\sqrt{2}}(p_z \pm ip_x), \quad d_\pm = \frac{1}{\sqrt{2}}(d_{z^2-x^2} \pm id_{zx}). \tag{1}$$

These are called the p-wave and d-wave, respectively. These are modes with a phase change of 2π in one cycle (optical vortex with charge number $l = \pm 1$) and 4π in one cycle (optical vortex with charge number $l = \pm 2$), respectively.

Generally, the center of the bandgap of each photonic structure is matched to the wavelength (frequency) of the light propagating through the topological waveguide, and therefore the transition ratio of the electromagnetic mode ($p_\pm$, $d_\pm$) is the same for all band diagrams. Consequently, the optical vortex modes with $l = \pm 1$ and $l = \pm 2$ propagating through the topological waveguide are mixed in a ratio of 1:1. When optical vortices are used to realize multiplexing technology, it is generally necessary to handle mutually perpendicular optical vortex signals with specific charge numbers. Hence, in optical circuits, it is essential to selectively propagate only optical vortex modes with a specific charge number l rather than the abovementioned mixed optical vortex modes.

Therefore, as shown in Figs. 1(b) and 1(c), we consider the situation in which the band diagrams of the two photonic structures that comprise the topological waveguide are shifted in opposite directions. In this case, when the lower bandgap edge of the trivial photonic structure and the upper bandgap edge of the topological photonic structure are brought close to the target light wavelength, the transition of the $p_\pm$ electromagnetic mode becomes dominant compared to that of the $d_\pm$ electromagnetic mode [Fig. 1(b)]. Therefore, the optical vortex mode that propagates through the topological waveguide consisting of these two photonic structures is limited to the mode with $l = \pm 1$. Similarly, when the upper bandgap edge of the trivial photonic structure and the lower bandgap edge of the topological photonic structure are brought close to the target light wavelength, the transition of the $d_\pm$ electromagnetic mode becomes dominant [Fig. 1(c)]. In this case, the topological waveguide only allows the optical vortex mode with $l = \pm 2$. It should be noted that these phenomena are unique to cases in which the used photonic structures have $\mathbb{Z}2$ topology.

We examined the possibility that each topological waveguide is able to select the appropriate optical vortex mode using the method described in the preceding paragraph. First, a photonic structure with band diagrams as explained in Figs. 1(b) and 1(c) was designed. In this study, a structure in which nanoholes were

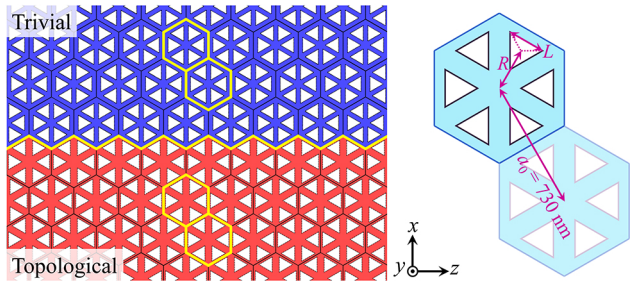

Fig. 2. Topological photonic waveguide and lattice structure with $\mathbb{Z}2$ topology used in the simulation.

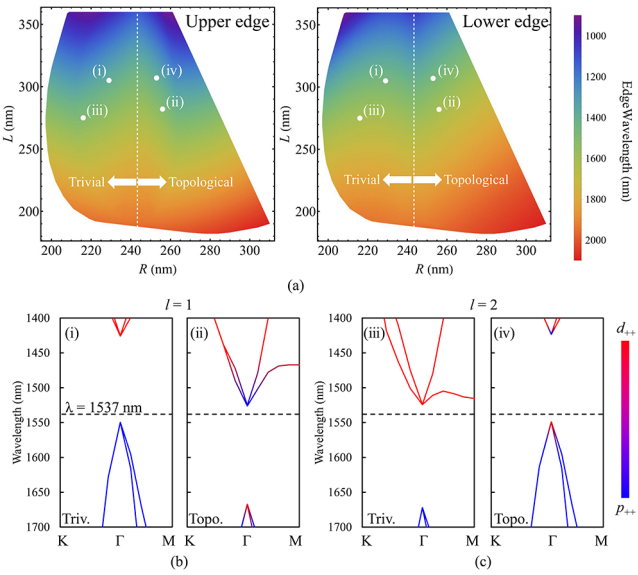

Fig. 3. (a) Theoretical results of the wavelengths (i.e., energies) of the upper and lower bandgap edges in the band diagram of each structure with different parameters. (b) Band diagrams of a photonic structure with $R = 229$ nm and $L = 305$ nm and a photonic structure with $R = 256$ nm and $L = 282$ nm. Only the optical vortex mode with $l = \pm 1$ can pass through a topological waveguide using these structures. (c) Band diagrams of a photonic structure with $R = 216$ nm and $L = 275$ nm and a photonic structure with $R = 253$ nm and $L = 307$ nm. Only the optical vortex mode with $l = \pm 2$ can pass through a topological waveguide using these structures.

arranged in a deformed honeycomb lattice with C_{6v} symmetry was used as the photonic structure with $\mathbb{Z}2$ topology (Fig. 2). The dielectric that constitutes the photonic structure was silicon [33] and the period of the honeycomb lattice a_0 was fixed at 730 nm. The distance from the center of the hexagonal unit cell to the center of the nanohole R and the length of the nanohole L were taken as parameters.

Figure 3(a) shows the results of the wavelengths (i.e., the energies) of the upper and lower bandgap edges in the band diagram of each structure according to the PWE method. Here, in the range $R = 245$–320 nm, the inversion of the p-wave and d-wave modes near the Γ point of the band diagram is observed, and the topology of the photonic structure changes. The respective topologically different structures are called the "trivial photonic structure" and the "topological photonic structure" satisfy the condition $a_0/R > 3$ and $a_0/R < 3$ [26]. In this case, because the width of the bandgap changes mainly according to the change

in R and the wavelength band of the bandgap changes according to the change in L, it is possible to obtain the desired bandgap by selecting R and L appropriately.

Using the results shown in Fig. 3(a), we selected four structures for realizing the concept shown in Fig. 1 and performed a detailed band analysis using the FDTD method. Figure 3(b) shows the results of combining the band diagrams of a trivial photonic structure with $R = 229$ nm and $L = 305$ nm and a topological photonic structure with $R = 256$ nm and $L = 282$ nm. The positional relationship of these structures with the target light wavelength (1537 nm) agrees with the relationship shown in Fig. 1(b). Additionally, Fig. 3(c) shows the results of combining the band diagrams for a trivial photonic structure with $R = 216$ nm and $L = 275$ nm and a topological photonic structure with $R = 253$ nm and $L = 307$ nm. The positional relationship of these structures with the target light wavelength (1537 nm) agrees with the relationship shown in Fig. 1(c). It is thought that by forming a topological waveguide using these structures,

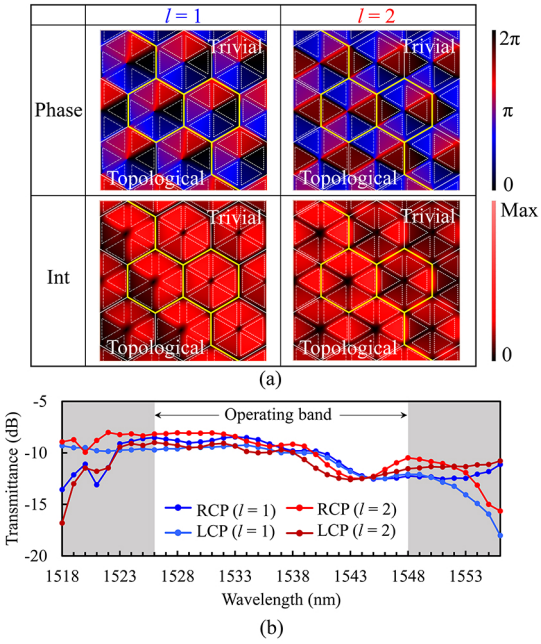

Fig. 4. (a) Calculated phase and intensity of the magnetic field (H_y) near a topological waveguide consisting of photonic structures with the band diagrams shown in Figs. 3(b) and 3(c) at a wavelength of 1540 nm (see Visualization 1, Visualization 2, Visualization 3, Visualization 4, Visualization 5, Visualization 6, Visualization 7, and Visualization 8). (b) Calculated propagation loss for each topological waveguide as a function of wavelength.

the transition of the $p_{\pm}$ (or $d_{\pm}$) electromagnetic mode becomes dominant, and it becomes possible to select the propagation of only the optical vortex mode with $l = \pm 1$ (or $l = \pm 2$). In this case, because the direct bandgap at Γ point is required to realize the topological edge state, the operation wavelength bands in Figs. 3(b) and 3(c) become 1526–1549 and 1524–1548 nm, respectively, and it is possible to cover a wide range within the C band.

Based on the abovementioned photonic structure, we analyzed the propagation characteristics of the topological waveguide created at the interface between trivial and topological photonic structures by the FDTD method. Figure 4(a) shows the phase and intensity of the magnetic field (H_y) of the propagating light at a wavelength of 1540 nm viewed directly above a topological waveguide consisting of photonic structures with the band diagrams shown in Figs. 3(b) and 3(c) (see Visualization 1, Visualization 2, Visualization 3, Visualization 4, Visualization 5, Visualization 6, Visualization 7, and Visualization 8 for the time variation). Enlarging the lattice in each topological waveguide, the propagating light has a phase change of 2π (optical vortex with charge $l = \pm 1$) and a phase change of 4π (optical vortex with charge $l = \pm 2$), respectively, which rotate over time. The results show that, for each structure, $l = 1$ and $l = 2$ are selected as the optical vortices propagating in the band-tuned topological waveguide. By separating each orthogonal vortex mode from the mode distribution in Fig. 4(a), the ratio of p-wave to d-wave (p-wave/d-wave) for $l = \pm 1$ and $l = \pm 2$ waveguides was estimated to be 10.11 and 0.0965, respectively. It should be noted that only the H_y component behaves like an optical vortex. The cross-sectional modes of the topological waveguide are the usual TE modes, and the energy flow is proceeding in the direction of the waveguide while their propagation direction changes in a complex manner at each local point.

Figure 4(b) shows the wavelength-dependent analysis results of the band-tuned topological waveguide. Here, in the wavelength range of 1526–1548 nm (which is an operation wavelength band of the topological waveguide), all waveguides have the same wavelength dependence, and the decrease in transmission intensity due to spin-spin scattering is observed at the wavelength of 1545 nm. On the other hand, in the wavelength range where the topological waveguide does not work, large fluctuations were confirmed because remarkable light leakage occurred outside the topological waveguides.

As one example, we designed the structure of an optical vortex and polarization demultiplexer by constructing a band-tuned topological waveguide on an optical circuit, and we analyzed its characteristics. Figures 5(a) and 5(b) show schematic views of the device. Here, the multiplexed signal incident on the center of the device is separated into four waveguides through regions

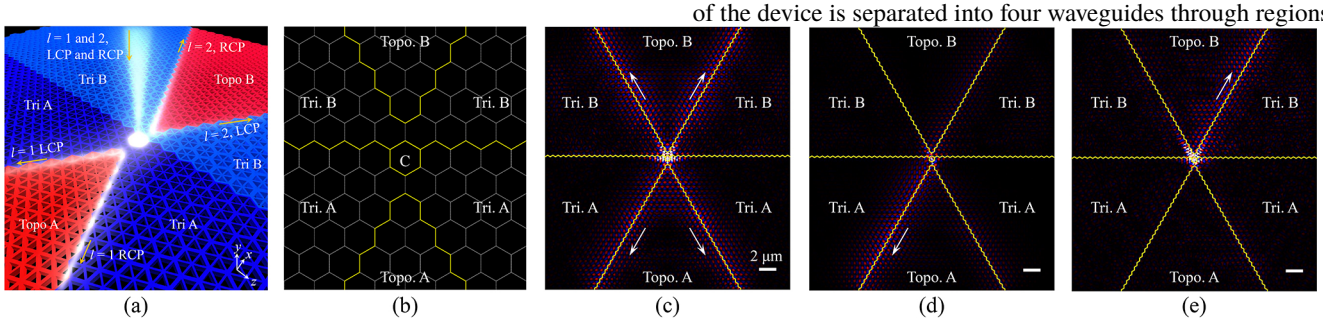

Fig. 5. (a) Optical vortex and polarization demultiplexer obtained by constructing a band-tuned topological waveguide. (b) Enlarged center of the device. (c) Calculated magnetic field distribution (H_y) when a signal multiplexed with all optical vortices and polarizations is used as input. (d), (e) Results obtained when left circularly polarized signals with $l = |1|$ and $|2|$ are used as inputs.

composed of photonic structures with four different band tunings. Based on the previous analysis, photonic structures of (R, L) = (229 nm, 305 nm), (256 nm, 282 nm), (216 nm, 275 nm), and (253 nm, 307 nm) were placed in the Tri A, Topo A, Tri B, and Topo B regions in Fig. 5(b), respectively. In addition, no nanoholes were placed in region C, and signals were inputted in this area. The optical vortices and polarizations used for multiplexing were the two types of charge numbers $l = |1|$ and $|2|$, right circular polarization (RCP) and left circular polarization (LCP), respectively.

Figures 5(c)–5(e) show the magnetic field distribution (H_y) calculated by the FDTD method. Figure 5(c) shows the result obtained when a signal multiplexed with all optical vortices and polarizations is the input. It can be seen that each signal with a particular optical vortex and polarization propagates to the corresponding output. Figures 5(d) and 5(e) show the results obtained when left circularly polarized signals with $l = |1|$ and $|2|$, respectively, were the inputs. It can be seen that an output was obtained only for a specific topological waveguide. This shows that by making good use of the characteristics of topological waveguides, completely passive and powerless optical vortex and polarization demultiplexing is possible, which will be very useful for future optical vortex multiplexing communications.

In this paper, we proposed a method for selectively propagating optical vortex modes with specific charge numbers in an optical circuit by using a topological photonic system. It is possible to selectively excite/propagate optical vortex modes with specific charge numbers in topological waveguides by performing appropriate band tuning in topological photonic crystals. The proposed method could be useful for controlling optical vortex signals in future orbital angular momentum multiplexing technologies.

Funding. Ministry of Internal Affairs and Communications (#182103111); Japan Society for the Promotion of Science (#19H02193, #21J14822); Core Research for Evolutional Science and Technology, Japan Science and Technology Agency (JPMJCR18T4).

Disclosures. The authors declare no conflicts of interest.

Data availability. Data underlying the results presented in this paper are not publicly available at this time but may be obtained from the authors upon reasonable request.

REFERENCES

1. G. Rademacher, B. J. Puttnam, R. S. Luís, J. Sakaguchi, W. Klaus, T. A. Eriksson, Y. Awaji, T. Hayashi, T. Nagashima, T. Nakanishi, T. Taru, T. Takahata, T. Kobayashi, H. Furukawa, and N. Wada, in *Optical Fiber Communication Conference (OFC) 2020*, OSA Technical Digest (2020), paper Th3H.1.
2. B. J. Puttnam, R. S. Luís, G. Rademacher, Y. Awaji, and H. Furukawa, in *Optical Fiber Communication Conference (OFC) 2021*, OSA Technical Digest (2021), paper F3B.3.
3. L. Allen, M. W. Beijersbergen, R. J. C. Spreeuw, and J. P. Woerdmanet, Phys. Rev. A **45**, 8185 (1992).
4. X. Cai, J. Wang, M. J. Strain, B. Johnson-Morris, J. Zhu, M. Sorel, J. L. O'Brien, M. G. Thompson, and S. Yu, Science **338**, 363 (2012).
5. R. C. Devlin, A. Ambrosio, D. Wintz, S. L. Oscurato, A. Y. Zhu, M. Khorasaninejad, J. Oh, P. Maddalena, and F. Capasso, Opt. Express **25**, 377 (2017).
6. Y. Shen, X. Wang, Z. Xie, C. Min, X. Fu, Q. Liu, M. Gong, and X. Yuan, Light: Sci. Appl. **8**, 90 (2019).
7. J. Wang, J.-Y. Yang, I. M. Fazal, N. Ahmed, Y. Yan, H. Huang, Y. Ren, Y. Yue, S. Dolinar, M. Tur, and A. E. Willner, Nat. Photonics **6**, 488 (2012).
8. N. Bozinovic, Y. Yue, Y. Ren, M. Tur, P. Kristensen, H. Huang, A. E. Willner, and S. Ramachandran, Science **340**, 1545 (2013).
9. J. Wang, Photonics Res. **4**, B14 (2016).
10. T. Lei, M. Zhang, Y. Li, P. Jia, G. N. Liu, X. Xu, Z. Li, C. Min, J. Lin, C. Yu, H. Niu, and X. Yuan, Light: Sci. Appl. **4**, e257 (2015).
11. M. Lavery, C. Peuntinger, K. Günthner, P. Banzer, D. Elser, R. Boyd, M. Padgett, C. Marquardt, and G. Leuchs, Sci. Adv. **3**, e1700552 (2017).
12. L. Li, R. Zhang, Z. Zhao, G. Xie, P. Liao, K. Pang, H. Song, C. Liu, Y. Ren, G. Labroille, P. Jian, D. Starodubov, B. Lynn, R. Bock, M. Tur, and A. E. Willner, Sci. Rep. **7**, 17427 (2017).
13. L. Zhu, A. Wang, S. Chen, J. Liu, Q. Mo, C. Du, and J. Wang, Opt. Express **25**, 25637 (2017).
14. Z. Xie, S. Gao, T. Lei, S. Feng, Y. Zhang, F. Li, J. Zhang, Z. Li, and X. Yuan, Photonics Res. **6**, 743 (2018).
15. T. Amemiya, T. Yoshida, Y. Atsumi, N. Nishiyama, Y. Miyamoto, Y. Sakakibara, and S. Arai, in *Optical Fiber Communication Conference (OFC)* , OSA Technical Digest (2019), paper M1C.7.
16. J. Kang, Y. Atsumi, Y. Hayashi, J. Suzuki, Y. Kuno, T. Amemiya, N. Nishiyama, and S. Arai, Appl. Phys. Express **7**, 032202 (2014).
17. T. Komljenovic, M. Davenport, J. Hulme, A. Y. Liu, C. T. Santis, A. Spott, S. Srinivasan, E. J. Stanton, C. Zhang, and J. E. Bowers, J. Lightwave Technol. **34**, 20 (2016).
18. K. Itoh, Y. Kuno, Y. Hayashi, J. Suzuki, N. Hojo, T. Amemiya, N. Nishiyama, and S. Arai, IEEE J. Sel. Top. Quantum Electron. **22**, 255 (2016).
19. R. Jones, P. Doussiere, J. B. Driscoll, W. Lin, H. Yu, Y. Akulova, T. Komljenovic, and J. E. Bowers, IEEE Nanotechnology Mag. **13**, 17 (2019).
20. Y. Jiao, N. Nishiyama, J. van der Tol, J. van Engelen, V. Pogoretskiy, S. Reniers, A. A. Kashi, Y. Wang, V. D. Calzadilla, M. Spiegelberg, Z. Cao, K. Williams, T. Amemiya, and S. Arai, Semicond. Sci. Technol. **36**, 013001 (2020).
21. T. Amemiya, K. Saito, H. Kagami, S. Okada, and X. Hu, "Topological photonic circuit," *U.S. Patent application*.
22. H. Kagami, T. Amemiya, S. Okada, N. Nishiyama, and X. Hu, Opt. Express **28**, 33619 (2020).
23. H. Kagami, T. Amemiya, S. Okada, N. Nishiyama, and X. Hu, Opt. Express **29**, 32755 (2021).
24. M. Hafezi, S. Mittal, J. Fan, A. Migdall, and J. M. Taylor, Nat. Photonics **7**, 1001 (2013).
25. L. Lu, J. D. Joannopoulos, and M. Soljačić, Nat. Photonics **8**, 821 (2014).
26. L.-H. Wu and X. Hu, Phys. Rev. Lett. **114**, 223901 (2015).
27. A. B. Khanikaev and G. Shvets, Nat. Photonics **11**, 763 (2017).
28. M. Segev and M. A. Bandres, Nanophotonics **10**, 425 (2020).
29. Y. Yang, Y.-F. Xu, T. Xu, H.-X. Wang, J.-H. Jiang, X. Hu, and Z.-H. Hang, Phys. Rev. Lett. **120**, 217401 (2018).
30. N. Parappurath, F. Alpeggiani, L. Kuipers, and E. Verhagen, Sci. Adv. **6**, eaaw4137 (2020).
31. J. Ma, X. Xi, and X. Sun, Adv. Mater. **33**, 2006521 (2021).
32. S. Iwamoto, Y. Ota, and Y. Arakawa, Opt. Mater. Express **11**, 319 (2021).
33. C. D. Salzberg and J. J. Villa, J. Opt. Soc. Am. **47**, 244 (1957).